# Thermomechanical modeling of slab eduction

T. Duretz,[1,2] T. V. Gerya,[2] B. J. P. Kaus,[3] and T. B. Andersen[4]

[1] Plate eduction is a geodynamic process characterized by normal-sense coherent motion of previously subducted continental plate. This mechanism may occur after slab detachment has separated the negatively buoyant oceanic plate from the positively buoyant orogenic root. Eduction may therefore be partly responsible for exhumation of high pressure rocks and late orogenic extension. We used two-dimensional thermomechanical modeling to investigate the main features of the plate eduction model. The results show that eduction can lead to the quasi adiabatic decompression of the subducted crust ($\approx 2$ GPa) in a timespan of 5 My, large localized extensional strain in the former subduction channel, flattening of the slab, and a topographic uplift associated with extension of the orogen. In order to further investigate the forces involved in the eduction process, we ran systematic parametric simulations and compared them to analytic plate velocity estimations. These experiments showed that eduction is a plausible mechanism as long as the viscosity of the asthenospheric mantle is lower than $10^{22}$ Pa.s while subduction channel viscosity does not exceed $10^{21}$ Pa.s. We suggest that eduction can be a viable geodynamic mechanism and discuss its potential role during the orogenic evolution of the Norwegian Caledonides.

**Citation:** Duretz, T., T. V. Gerya, B. J. P. Kaus, and T. B. Andersen (2012), Thermomechanical modeling of slab eduction, *J. Geophys. Res.*, *117*, B08411, doi:10.1029/2012JB009137.

## 1. Introduction

### 1.1. Background

[2] The exhumation of high pressure and ultra high pressure (HP-UHP) metamorphic rocks at convergent margins is a very active field of research in tectonics and geodynamics. Understanding the long term dynamics of subduction-collision zones requires conceptual models, which can account for both real Earth geological and geophysical observations and comply with quantitative geomechanical models.

[3] Numerous models specifically focused on the processes driving the exhumation of HP-UHP rocks are available in the literature. Syn-to-late collisional exhumation models involve mechanisms such as corner flow or buoyant flow within the subduction channel [*Cloos and Shreve*, 1988; *Gerya et al.*, 2002; *Yamato et al.*, 2008; *Li and Gerya*, 2009], buoyancy driven crustal stacking and development of normal sense shear zones [*Chemenda et al.*, 1995, 1996], crustal flow associated with the gravitational spreading of orogens [*Andersen and Jamtveit*, 1990; *Vanderhaeghe and Teyssier*, 2001] and focused

erosion [*Beaumont et al.*, 2001, 2004, 2006], slab rollback driven by the retreat of the subducting slab [*Lister et al.*, 2001; *Schellart et al.*, 2006; *Brun and Facenna*, 2008; *Husson et al.*, 2009; *Bialas et al.*, 2011] and delamination of the crust [*Bird*, 1978], or slab extraction involving slab detachment and the decompression of buried material by plate unbending [*Froitzheim et al.*, 2003; *Janák et al.*, 2006].

[4] The slab detachment model necessitates the build up tensional stresses that overcomes the strength of the subducting plate. Such scenario is likely to take place during an attempted ridge subduction or a continental crust subduction/collision. Both of these contexts have been subject to extensive two-dimensional studies [*Davies and von Blanckenburg*, 1995; *Buiter et al.*, 2002; *Andrews and Billen*, 2009; *Baumann et al.*, 2009; *Duretz et al.*, 2011] as well as three-dimensional modeling [*Burkett and Billen*, 2011; *van Hunen and Allen*, 2011] and analytical studies focused on necking dynamics [*Schmalholz*, 2011]. All models agree on the fact that slab detachment causes a dramatic change in the orogenic force balance. Yet, the dynamic consequences of this force balance perturbation have not yet been studied in detail.

### 1.2. The Term "Eduction"

[5] The concept of plate eduction has been introduced by *Dixon and Farrar* [1980] to describe a mechanism that could lead to the exhumation of subducted/accreted rocks at an ocean-continent margin. Their model, conceived for the exhumation of the Californian Franciscan blueschists, involved the subduction of an actively spreading ridge beneath North America. The subduction of a ridge triggers shallowing of the slab and the ongoing spreading promotes extension in the subducting slab which would eventually

[1]ISTEP, UMR 7193, UPMC Paris 06, CNRS, Paris, France.
[2]Department of Earth Sciences, Institute of Geophysics, ETH Zürich, Zürich, Switzerland.
[3]Institute of Geosciences, Johannes Gutenberg University Mainz, Mainz, Germany.
[4]Physics of Geological Processes, University of Oslo, Oslo, Norway.

Corresponding author: T. Duretz, Department of Earth Sciences, Institute of Geophysics, ETH Zürich, Sonneggstr. 5, Zürich CH-8092, Switzerland. (Thibault.Duretz@erdw.ethz.ch)
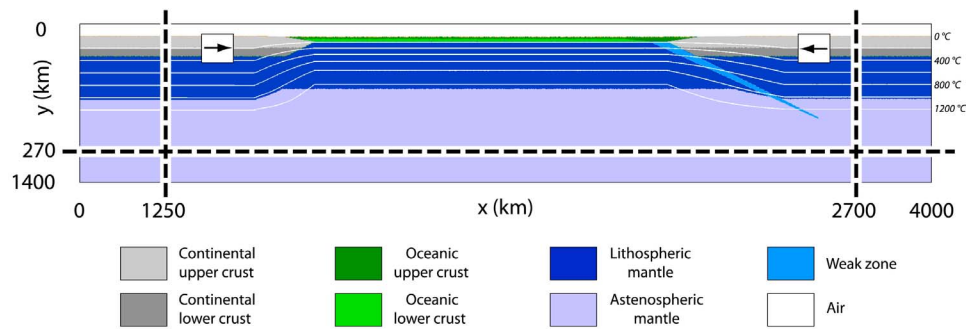
**Figure 1.** Initial distribution of the compositional fields employed in the continental collision experiments. The initial thermal age of the slab is 40 My. The arrows indicate the location where the push condition is initially applied. A total convergence rate of 5 cm/y is imposed until 500 km of convergence has been reached.

lead to the exhumation of the subducted/accreted material along the margin.

[6] *Andersen et al.* [1991] introduced the subduction-eduction model to explain burial and exhumation of HP-UHP rocks in continent-continent collision. Based on geological data from one the largest and best preserved HP-UHP provinces in the world this work highlighted the potential link between slab detachment, orogenic extension and exhumation of coherent slab of HP-UHP rocks through the evolution of the Norwegian Caledonides. In this model, the continental lithosphere was subducted to the point at which slab detachment occurred, causing the removal of the slab pull force. Subsequently, the subducted and vertically stretched continental plate was coherently educted leading to the exhumation of HP-UHP rocks along a large normal-sense shear zone near the former subduction plane. This eduction concept has remained a popular model in the literature focused on postorogenic extension, specifically for the case of the Caledonides [*Fossen*, 2000; *Brueckner and van Roermund*, 2004; *Brueckner*, 2009; *Rey et al.*, 1997; *Schlindwein and Jokat*, 2000] and the Variscides [*Schneider et al.*, 2006]. This definition contrast with that of [*Dixon and Farrar*, 1980] since it explicitly implies a period of reversed subduction following slab detachment during continental collision.

### 1.3. Present Work

[7] In this paper we concentrate on the large scale geodynamic process of lower plate eduction in a continental collisional context (i.e. definition of *Andersen et al.* [1991]). Post slab detachment eduction was observed in several previous numerical modeling studies [*Mishin et al.*, 2008; *Duretz et al.*, 2011] but has not yet been subjected to a systematic parametric study. We therefore focus on the description of the major features of the eduction model and study its dynamics by means of two-dimensional numerical modeling. Finally, we discuss the potential role of eduction for the exhumation of HP-UHP rocks and focus on the case of the Norwegian Caledonides.

## 2. Numerical Modeling

### 2.1. Setup

[8] We have used a setup consisting of two continents and of, initially, one ocean (Figure 1). The simulations were run with the thermomechanical code I2VIS [*Gerya and Yuen*, 2003a], a description of the code is provided in Appendix A. Each lithology was characterized by a temperature-stress dependent visco-plastic rheology, with rheological and flow parameters as listed in Table 1. Following the approach of *Gerya et al.* [2004], all simulations included the effect of phases changes on material densities neglecting the effects of reaction kinetics. The size of the model domain was $4000 \times 1400$ km and variable grid spacing ($1361 \times 351$ nodes) was employed to attain a 1 km grid spacing in the collision area. We initially imposed a plate convergence rate of 5 cm/y by prescribing velocities inside the domain. As soon as the

**Table 1.** Thermal and Rheological Parameters for the Lithologies Employed in the Simulations[a]

| Material | k (W/m/K) | $H_r$ (W/m³) | $C_p$ (J/kg) | Flow Law | $\eta_0$ (Pa$^n$.s) | n | $E_a$ (J) | $V_a$ (J/bar) | $\sin(\phi)$ | C (MPa) |
|---|---|---|---|---|---|---|---|---|---|---|
| Sediments | $0.64 + \frac{807}{T+77}$ | $1.50 \times 10^{-6}$ | 1000 | wet Qz. | $1.97 \times 10^{17}$ | 2.3 | $1.54 \times 10^5$ | 0.8 | 0.15 | 1 |
| Upper cont. crust | $0.64 + \frac{807}{T+77}$ | $1.00 \times 10^{-6}$ | 1000 | wet Qz. | $1.97 \times 10^{17}$ | 2.3 | $1.54 \times 10^5$ | 0.8 | 0.15 | 1 |
| Lower cont. crust | $1.18 + \frac{474}{T+77}$ | $0.25 \times 10^{-6}$ | 1000 | Pl. (An75) | $4.80 \times 10^{22}$ | 3.2 | $2.38 \times 10^5$ | 1.2 | 0.15 | 1 |
| Upper oceanic crust | $0.64 + \frac{807}{T+77}$ | $0.25 \times 10^{-6}$ | 1000 | wet Qz. | $1.97 \times 10^{17}$ | 2.3 | $1.54 \times 10^5$ | 0.8 | 0.00 | 1 |
| Lower oceanic crust | $1.18 + \frac{474}{T+77}$ | $0.25 \times 10^{-6}$ | 1000 | Pl. (An75) | $4.80 \times 10^{22}$ | 3.2 | $2.38 \times 10^5$ | 0.8 | 0.60 | 1 |
| Mantle | $0.73 + \frac{1293}{T+77}$ | $2.20 \times 10^{-8}$ | 1000 | dry Ol. | $3.98 \times 10^{16}$ | 3.5 | $5.32 \times 10^5$ | 0.8 | 0.60 | 1 |
| Weak zone | $0.73 + \frac{1293}{T+77}$ | $2.20 \times 10^{-8}$ | 1000 | wet Ol. | $5.01 \times 10^{20}$ | 4.0 | $4.70 \times 10^5$ | 0.8 | 0.00 | 1 |

[a]Here k is the thermal conductivity, $H_r$ is the radiogenic heat production, $C_p$ is the specific heat capacity, $\eta_0$ is the reference viscosity, n is the stress exponent, $E_a$ is the activation energy, $V_a$ is the activation volume, $\phi$ is the internal friction angle, and C is the cohesion. Qz., Pl., and Ol. respectively stands for Quartzite, Plagioclase, and Olivine.
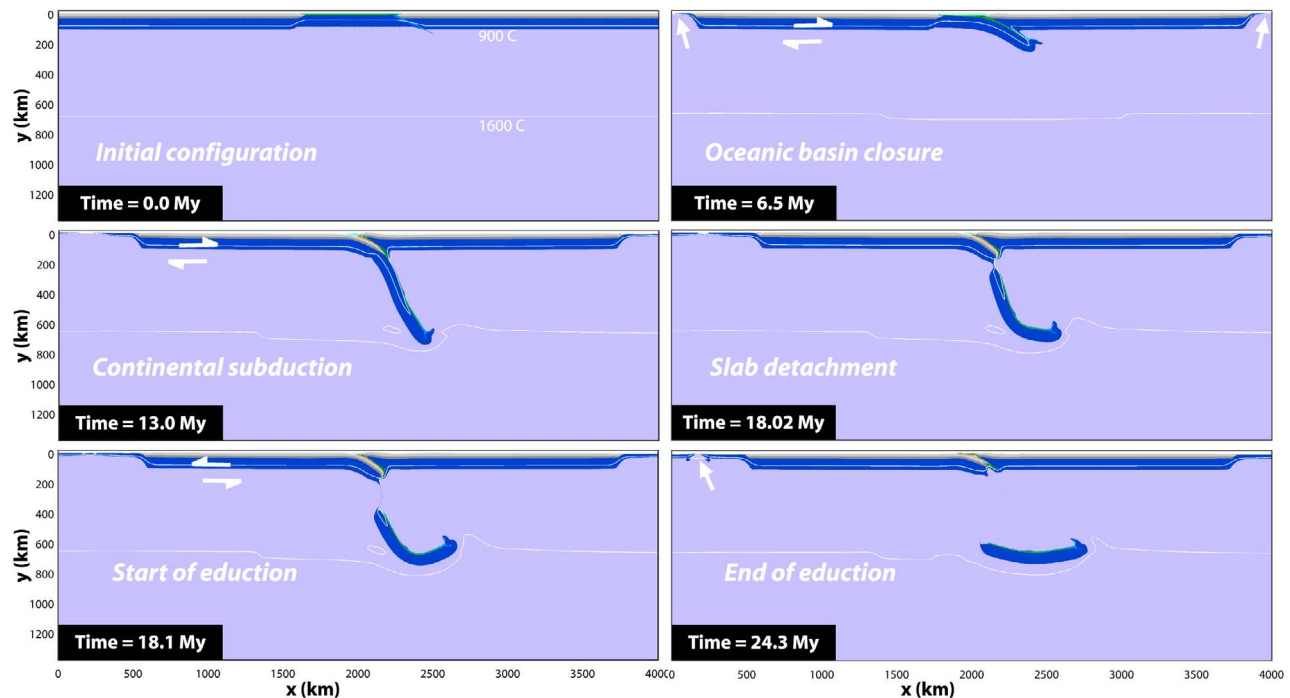
**Figure 2.** Large scale time evolution of the reference subduction/collision model. The two plates converge toward each other leaving space for the development of ridges in the vicinity of the model's left/right boundaries. The interaction of the detached slab with the 660 km phase boundary is also depicted.

model reached 500 km of convergence, the kinematic condition was deactivated and the models were subsequently driven by internal forces (e.g. slab pull). All the boundaries of the box were free slip. An additional, 20 km thick layer of sticky air ($\rho_{air} = 0$ kg/m$^3$, $\eta_{air} = 10^{18}$ Pa.s) was utilized in order to mimic the effect of a free surface and the development of topography [*Schmeling et al.*, 2008; *Crameri et al.*, 2012]. The setup was designed such that the continental plates detach from the sides of the box during convergence, leaving space for the development of oceanic ridges in the vicinity of the domain boundaries (see Figure 2). In the simulations presented here, the initial continental crustal thickness was 35 km. We do not vary this parameter in this study, nevertheless we expect that variations in crustal thickness (and therefore of plate buoyancy) will affect both the burial depth of the continental crust and the amount of subsequent eduction that can be accommodated.

### 2.2. Potential Causes for Eduction

[9] We assume that the closure of an oceanic basin occurs prior to continental collision and that this closure stage is accommodated by oceanic plate subduction. Depending on the dimensions, convergence rate and density structure of the oceanic basin, subduction generates the slab pull force which is generally considered as a major tectonic force [*Turcotte and Schubert*, 1982]. While continental margins enter into contact, a period of continental subduction can occur. Due to the buoyant nature of the crust, continental subduction is not steady and might terminate by slab detachment. Once slab detachment has occurred, and assuming a competent crustal rheology, the subducted continental

lithosphere may exhume coherently due its buoyancy triggering plate eduction. As presented in *Duretz et al.* [2011], plate eduction is likely to occur for continental collision involving relatively fast plate velocities (5–10 cm/y) and initial slab thermal ages ranging between 40 and 60 My. Younger slabs are too weak and detach before any continental crust subduction happens. Older slabs lead to a collisional regime dominated by retreat and delamination in the sense of *Bird* [1978]. It is important to notice that, in these models, eduction develops because no convergent kinematic constrains are imposed during the collision. Although the plates are laterally confined by newly formed oceanic lithosphere, the buoyancy of the root may be sufficiently large to overcome the ridge push force leading to divergent plate motion and inversion of the subduction plane.

## 3. The Plate Eduction Model: Reference Model

### 3.1. Time Evolution

[10] The model evolution can be decomposed in several successive stages (Figures 2 and 3). The earliest stage is the closure of the oceanic basin. During this period the slab pull ($F_P$) builds up progressively as oceanic plate subduction proceeds (Figure 4b). After 11 My, continental subduction initiates and continues until the ocean-continent transition (OCT) reaches a depth at which the positive buoyancy of the crust ($F_B$) compensates the negative buoyancy of the slab ($F_P \approx F_B \approx 3 \times 10^{13}$ N/m). This period lasts approximately 6.5 My and the OCT is buried to a maximum depth of 170 km. Slab detachment eventually occurs and necking takes place at the OCT separating the negative (oceanic) from
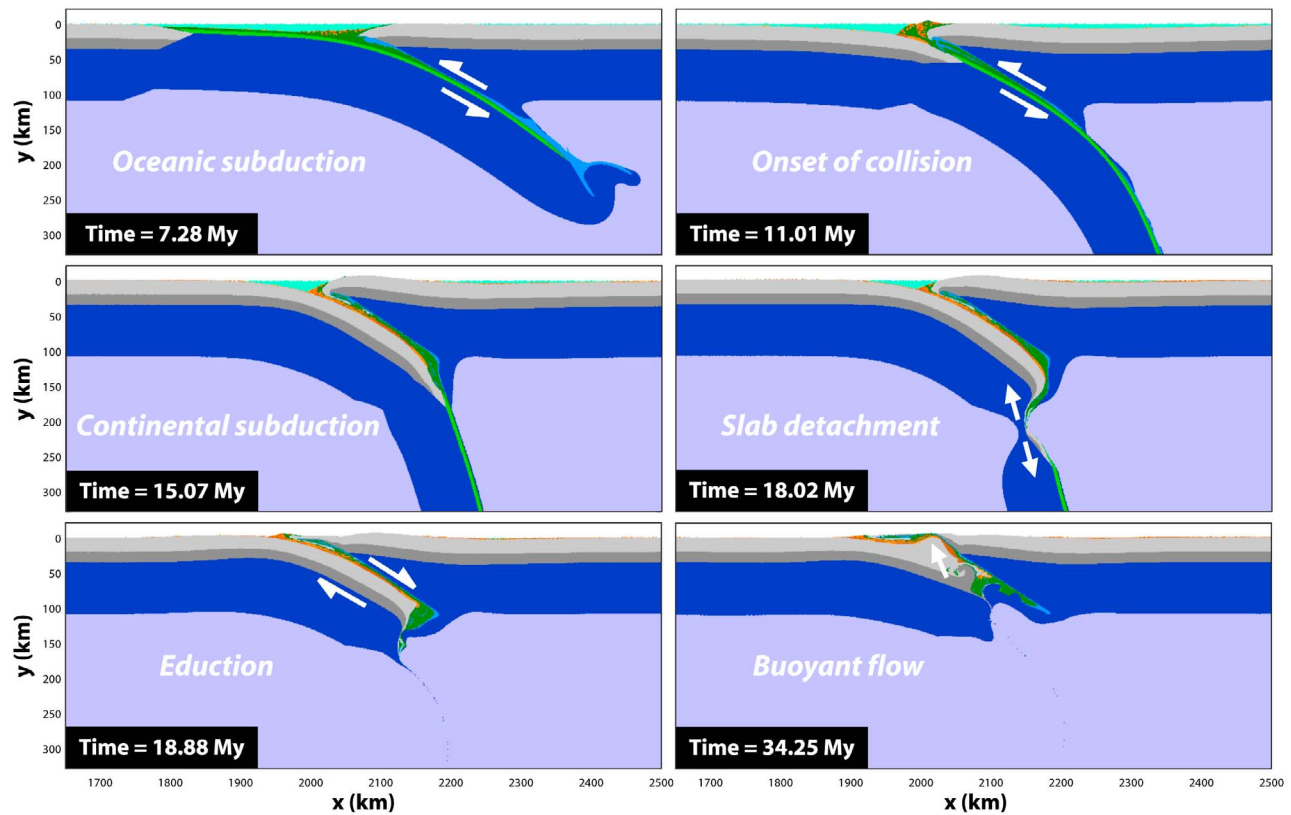
**Figure 3.** Time evolution of the plate eduction model in six stages focused on the collision zone. The white arrows highlight the sense of shear on the subduction plane, the stretching direction of the slab during detachment and the direction of flow during late exhumation. In this figure, the time is incremented from the start of the experiment. The orange/brown layers represents sediments that are deposited with ongoing subsidence.

the positively buoyant (continental) portions of the slab. Figure 4c show the average density difference between the subducted continental lithosphere and the surrounding asthenosphere. This density contrast is responsible for the build up of buoyant stress within the subducted crust and the large magnitude of the root buoyancy force. After the oceanic slab has detached, the slab pull force decreases dramatically (Figure 4b) and the system is driven by the continental root buoyancy and the ridge push ($\approx 1 - 5 \times 10^{12}$ N/m in our models). As a result of the imbalance between these two forces, the subduction plane reverses as a normal-sense shear zone along which the positive buoyancy of the subducted crust is accommodated. Throughout the eduction stage that lasts 5 My, the main portion of the slab returns toward the surface in a coherent motion. After a progressive decrease of the root buoyancy force (Figure 4b), the orogen is eventually affected by a period of buoyant flow which causes the continental crust to rise diapirically toward the surface of the model (see Figure 3).

### 3.2. Exhumation of the Subducted Crust

[11] In this model the exhumation occurs by two different mechanisms: plate eduction and buoyant flow. Eduction allows for a vertical displacement of the tip of the slab of about 60 km. Buoyant flow of the crust overtakes eduction at its latest stage and is responsible for doming at shallow structural level. These two exhumation stages are clearly identifiable on the pressure-temperature-time (PTt) paths of material tracers (Figure 5). These clockwise paths display a pressure peak corresponding to timing of slab detachment followed by a nearly adiabatic decompression corresponding to the eduction stage. The later cooling event occurs when buoyant flow takes over eduction, this process occurs at a crustal level (depth < 35 km). The signal of slab detachment, and subsequent eduction, can also be noticed on the vertical velocity ($v_y$) evolution of the material tracers (Figure 5). Slab detachment is followed by an "instantaneous" peak exhumation rate of 8 cm/y that exponentially decreases to a rate of about 0.8 cm/y through the period of eduction.

### 3.3. Topographic Evolution

[12] Plate eduction is responsible for a major uplift event or rebound following slab detachment. The topographic evolution of the subduction-collision zone can be divided in four geodynamic phases that are characterized by a specific surface imprint (Figure 6a). During the first 11 My period, closure of the oceanic basin takes place, collision takes over oceanic subduction and lasts until 18 My when slab
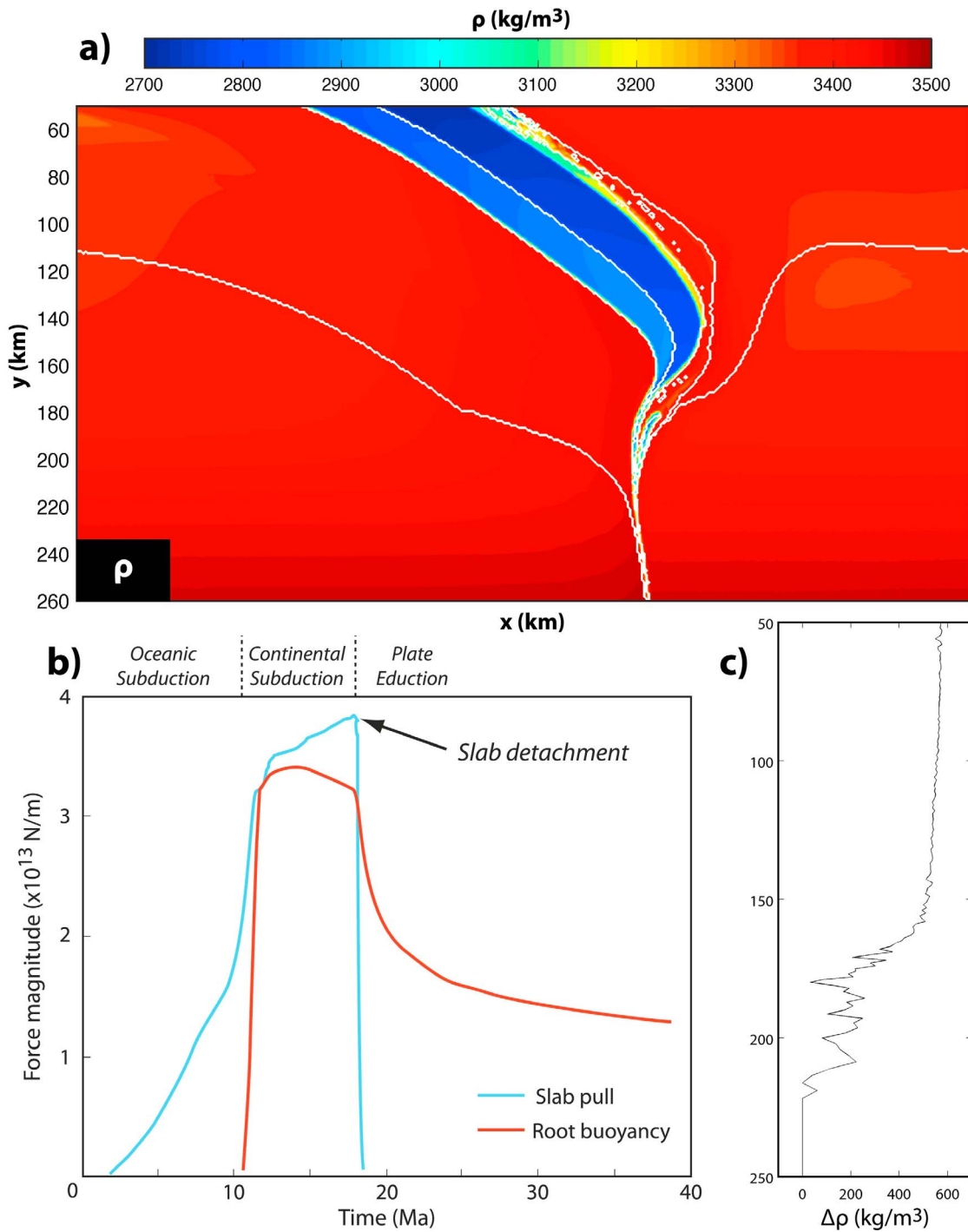
**Figure 4.** (a) Post slab detachment density structure. The white contours denotes lithological groups (sediments, upper crust, lower crust, mantle lithosphere and asthenosphere). (b) Time evolution of slab pull and root buoyancy forces (buried continental crust) throughout the subduction/collision history. The time is incremented from the onset of the experiment. (c) Average vertical profile of density difference between the subducted continental lithosphere and the asthenosphere after slab detachment. This average density contrast ($\Delta\rho$) is computed by first evaluating mean mantle and crust densities at each depth level (i.e. horizontal gridlines), and by subtracted one from the other.

detachment happens. While continental subduction proceeds, the topographic peak is located on the upper plate whereas a deep subduction trench is located on the lower plate. During the next 6 My following slab detachment, the topography builds up on both sides of the suture marking the stage of plate eduction. The uplift also takes place in the neighboring foreland and hinterland basins. The smooth transition between eduction and buoyant flow that occurs at around
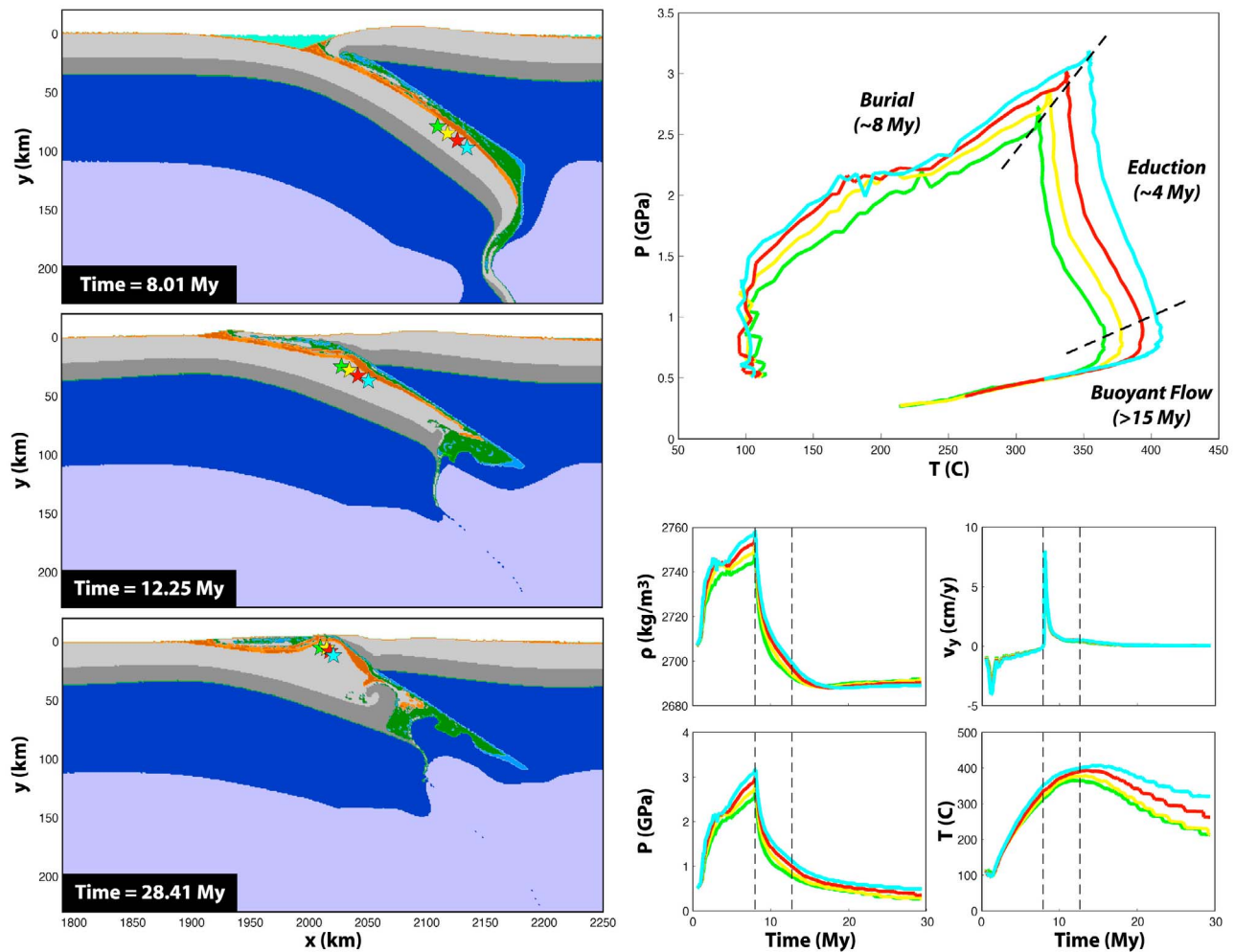
**Figure 5.** Pressure, temperature, density, vertical velocity evolution for 4 Lagrangian material tracers located in the subducted crust. The left column represents the location of the markers throughout the exhumation period. Dashed lines indicate the signal corresponding to slab detachment/start of eduction and the end of the eduction/start of buoyant flow. The time is incremented from the onset of the collision.

25 My of model time does not result in a sharp topographic feature.

### 3.4. Plate Deformation and Motion

[13] Eduction is characterized by a rigid-body (or coherent) motion of the lower plate. The transition from a subduction-related plate motion to eduction is sharp and is depicted in Figure 6b. This divergent motion causes localized extension within the subduction channel. The finite deformation pattern (Figure 7), produced using the methodology of *Huet et al.* [2010], reveals the intensity of the strain that accumulated along the subduction channel and the asthenospheric mantle underlying the plate. This illustrates the coherent plate motion resulting from the slab pull loss and the absence of kinematic constrains. The educted plate itself does not undergo any significant internal deformation apart from the pervasive but not intense strain resulting from the unbending. The surface plate velocities also highlight the rigid motion of lower plate throughout the collision. After slab detachment, the lower plate reaches a velocity on the order of $-5$ cm/y during few My which coincides with eduction (Figure 6b).

### 3.5. Slab Unbending/Flattening

[14] Another feature of the eduction model is tendency for the lower plate to unbend throughout the eduction stage. Figure 6c depicts the evolution of the slab dip angle after slab detachment occurred, the slab dip is here defined as the angle between the interface separating the underthrusted continental crust and the subduction channel. The normal shear motion along the former subduction interface is accompanied by the unbending of the lower plate and the flattening of the slab. In our reference model, the dip of the slab decreases from $35°$ to about $22°$ through the extensional period (5 My timespan).

### 4. The Dynamics of Plate Eduction

[15] As described above, plate eduction is a dynamic consequence of the loss of slab pull subsequent to slab detachment. In order to investigate which parameters control the post slab detachment tectonic regime, we have combined both an analytic approach (Figure 8a) and a simplified 2D numerical model (Figure 8b). The analytic method enables
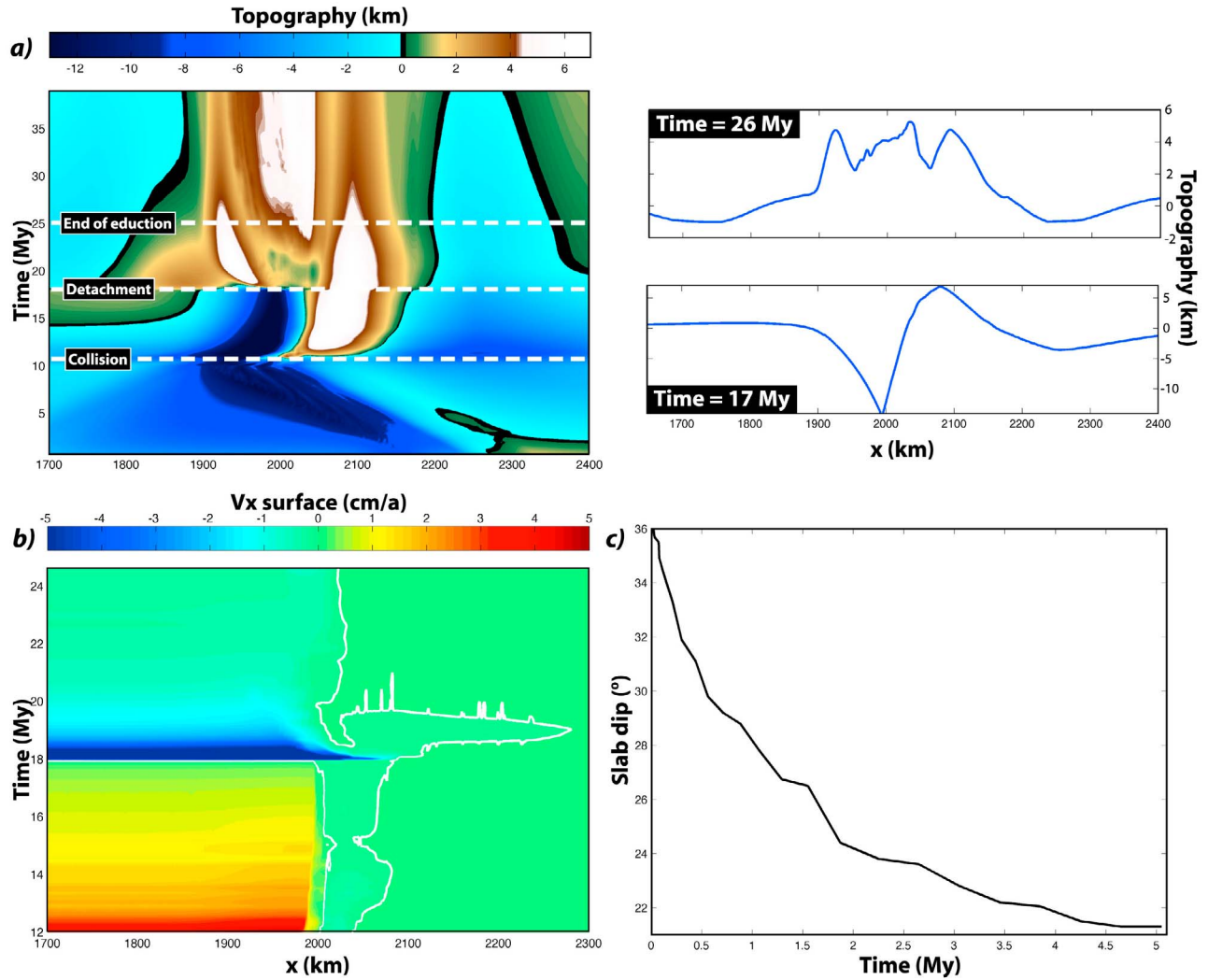
**Figure 6.** (a) Topographic evolution through time of the reference eduction model, white dashed lines indicate major geodynamic events affecting the topography. The two profiles on the right hand side display the topography along the collision zones before and after eduction. The time is incremented from the start of the experiment. (b) Horizontal plate velocity during continental subduction, slab detachment, and eduction. (c) Slab dip evolution through the period of eduction following slab detachment. The time axis origin is the timing of slab detachment.

to test the influence of the force difference acting on a plate whereas the numerical model allows for the independent variation of the orogenic root buoyancy and the ridge push force. These calculations are utilized to discriminate under which force regime subduction or eduction occurs.

## 5. A Corner Flow/Torque Balance Approach

[16] In order to obtain a first order prediction of subduction velocity we have used the classical torque balance approach [*Stevenson and Turner*, 1977; *Manea et al.*, 2006]. This approach is isoviscous and allows us to investigate the dependence of subduction velocity on the mantle viscosity and the slab angle. The torque balance formulates the equilibrium between the moments produced by gravity $M_G$ (i.e. slab's buoyancy) and mantle flow $M_F$ (i.e. "slab's lifting torque"). This simplistic approach neglects the torque related

to slab bending [*Dvorkin et al.*, 1993; *Lallemand et al.*, 2008].

[17] The hydrodynamic torque resulting from the arc and back arc pressures difference $(P_A - P_B)$ is obtained from the isoviscous stream function approach [*McKenzie*, 1969] expressed in polar co-ordinates $(r, \theta)$ and can be formulated as follows:

$$M_F = \int_0^L (P_A - P_B) r \delta r. \tag{1}$$

[18] The arc/back arc pressure difference is expressed as in [*Stevenson and Turner*, 1977]:

$$P_A - P_B = \frac{2\eta_{\text{ast}} V}{r} \left[ \frac{\sin \theta_s}{(\pi - \theta_s) + \sin \theta_s} + \frac{\sin^2 \theta_s}{\theta_s^2 - \sin^2 \theta_s} \right], \tag{2}$$
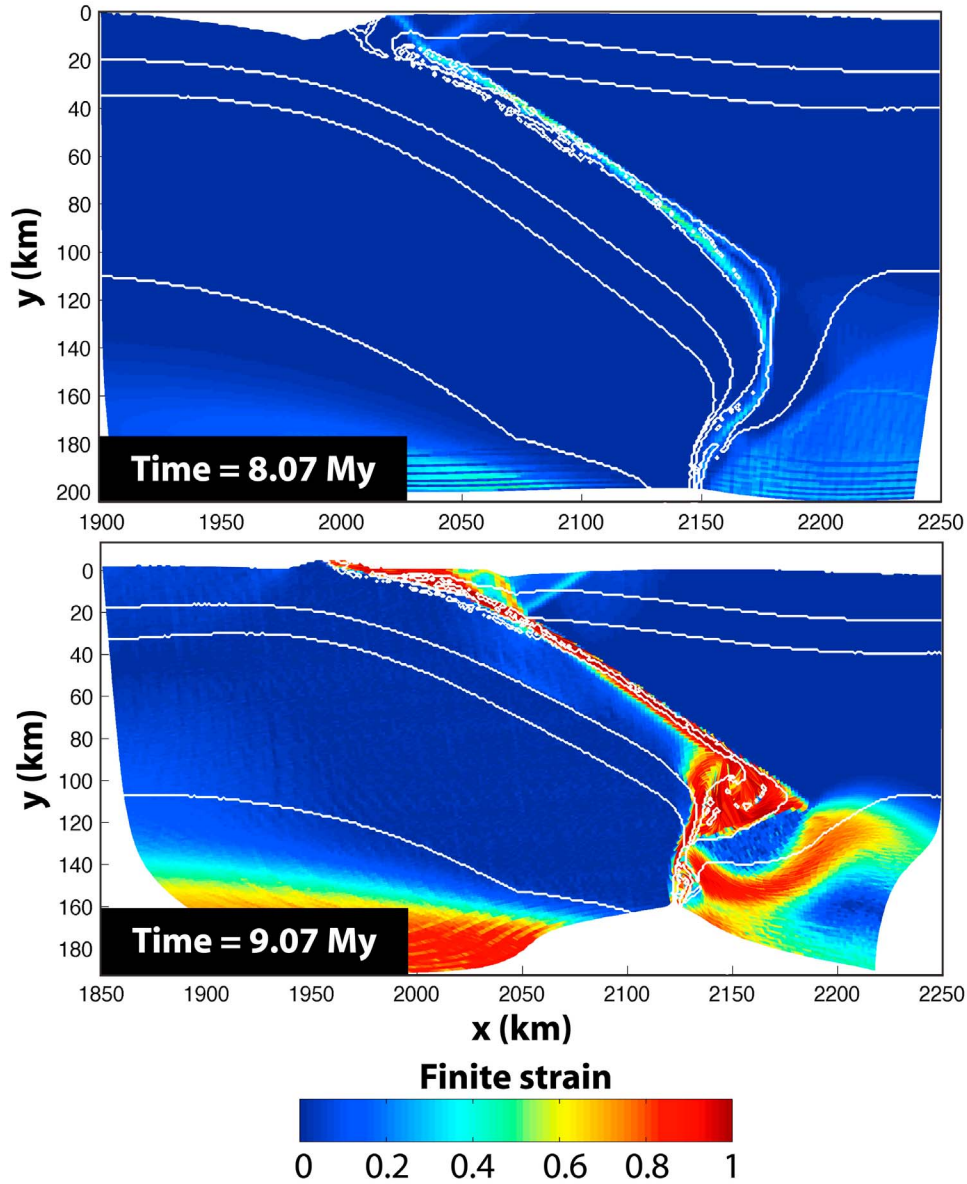
**Figure 7.** Finite strain intensity pattern related to eduction. Most of the deformation is accommodated by the subduction channel and the asthenosphere. The strain is incremented after the slab has detached. The time after collision has started is indicated. The white contours represent the interfaces between lithological groups (sediments, upper crust, lower crust, mantle lithosphere and asthenosphere).

where $\theta_s$ is the slab dip, $\eta_{\mathrm{ast}}$ is the asthenosphere viscosity, and V is the slab velocity. The gravitational torque results from the density difference existing between the slab and mantle ($\Delta\rho$):

$$M_G = \int_0^L \Delta\rho g h \cos\theta_s \, r\delta r, \qquad (3)$$

where $g$ and $h$ respectively stands for the gravitational acceleration and the slab thickness. Integrating and solving both expressions for $V$ leads to the velocity expression:

$$V = \frac{F\,K}{4\,\eta_{\mathrm{ast}}}, \qquad (4)$$

where $F = \Delta\rho g h L$ is the slab's buoyancy force and $K$ is a factor that depends on the slab dip:

$$K = \frac{\cos\theta_s}{\frac{\sin\theta_s}{(\pi-\theta_s)+\sin\theta_s} + \frac{\sin^2\theta_s}{\theta_s^2 - \sin^2\theta_s}}. \qquad (5)$$

[19] Assuming that the slab is rigid and transmits the far-field ridge push force, we may consider that the slab is effectively driven by the force difference between slab's buoyancy and ridge push acting in the direction of the slab ($F \propto dF = F_{\mathrm{P}}\cos\theta_s - F_{\mathrm{B}}\sin\theta_s$). Subsequently, the velocity expression can be rewritten as

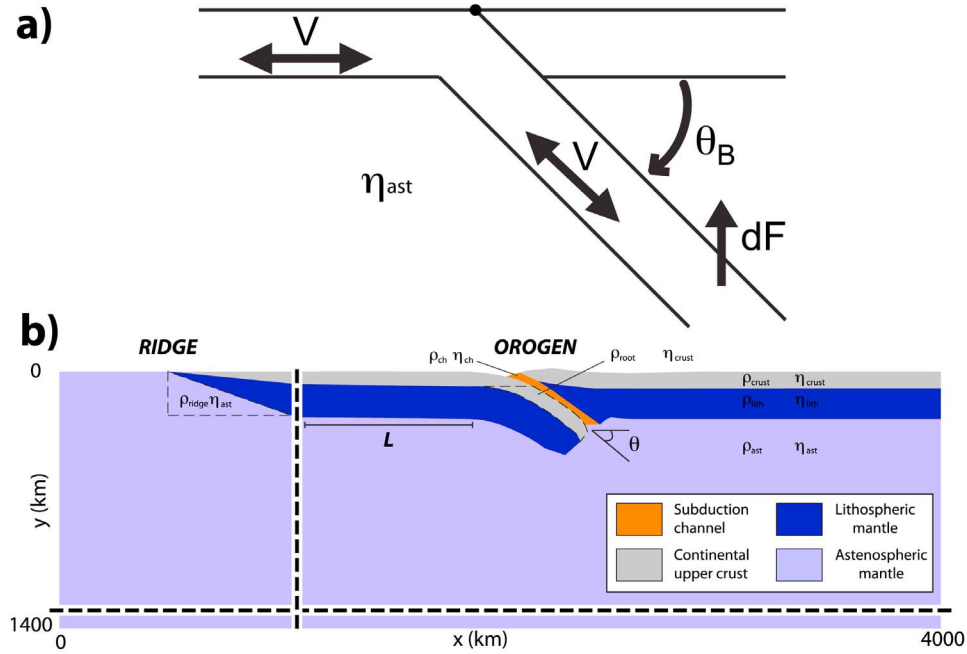$$V \propto \frac{dF\,K}{4\,\eta_{\mathrm{ast}}}, \qquad (6)$$

**Figure 8.** (a) Sketch of the corner flow/torque balance model used to calculated plate velocities. The plate is considered as rigid and the velocities are calculated from the balance between the gravitation torque and the hydrodynamic torque obtained from the corner flow model. (b) Simplified setup of a post slab detachment configuration. This setup is used to systematically investigate the parameters that control horizontal plate velocity (subduction or eduction) by varying the ridge push and the orogenic root buoyancy as well as the asthenosphere and subduction channel viscosity, the lower plate length ($L$) and the subduction angle ($\theta$).

where the velocity of plate motion is directly proportional to $dF$ and which is either positive when subduction occurs or negative when eduction takes place.

## 6. Simplified 2D Setup

[20] In order to test the applicability of the torque balance approach, we performed additional numerical simulations for a simplified setup that consists of a rigid newtonian (high-viscosity) slab and a linear viscous mantle. The steady state equation of momentum and incompressibility are discretized using T2P1 elements and solved for the given distribution of density and viscosity, after which the resulting instantaneous flow pattern is used to determine whether the orogen is undergoing subduction ($V_{\text{plate}} > 0$) or eduction ($V_{\text{plate}} < 0$). The boundary conditions are set to free slip on the left, right and bottom boundaries, and a free surface condition is applied at the top of the box. All the simulations were run using the code MILAMIN_EP [*Kaus*, 2010]. An unstructured mesh was employed to finely resolve the subduction interface. This method allows for fast and robust computation of flow fields as required for parametric studies.

[21] The horizontal (i.e. ridge push) force is prescribed by varying the density gradient between the asthenosphere and the plate, whereas the root buoyancy force is controlled by the density difference between the buried crust and the surrounding mantle (Figure 8b). We define the magnitude of the ridge push force as

$$F_{\text{P}} = (\rho_{\text{lit}} - \rho_{\text{ridge}})A_{\text{ridge}}\ g, \qquad (7)$$

where $\rho_{\text{lit}}$, $\rho_{\text{ast2}}$, and $A_{\text{ridge}}$ respectively stand for the lithosphere density, the ridge and the ridge area. Similarly, we define the magnitude of the orogenic root buoyancy as:

$$F_{\text{B}} = (\rho_{\text{lit}} - \rho_{\text{root}})A_{\text{root}}\ g, \qquad (8)$$

where $\rho_{\text{root}}$ and $A_{\text{root}}$ correspond to the density and the area of buried continental crust and are calculated according to the magnitude of each force such as:

$$\rho_{\text{ridge}} = \rho_{\text{lit}} - \frac{F_{\text{P}}}{A_{\text{ridge}}\ g} \qquad (9)$$

$$\rho_{\text{root}} = \rho_{\text{lit}} - \frac{F_{\text{B}}}{A_{\text{root}}\ g}. \qquad (10)$$

The tectonic regime is therefore controlled by the forces that are applied to the plates and imposed via the density distribution. In contrast to the isoviscous torque balance described in 5, such setup enables to explore the effect of the subduction channel rheology on plate kinematics.

### 6.1. Parameters Controlling Eduction

[22] Over the many parameters that affect the velocity of the subducting or educting plates, we have focused on the dip angle of slab and the viscosities of both the asthenosphere and the subduction channel. Both torque balance and 2D finite element (FE) models were employed to calculate plates velocity after slab detachment (the results are depicted in Figure 9a). Despite the different assumptions made with
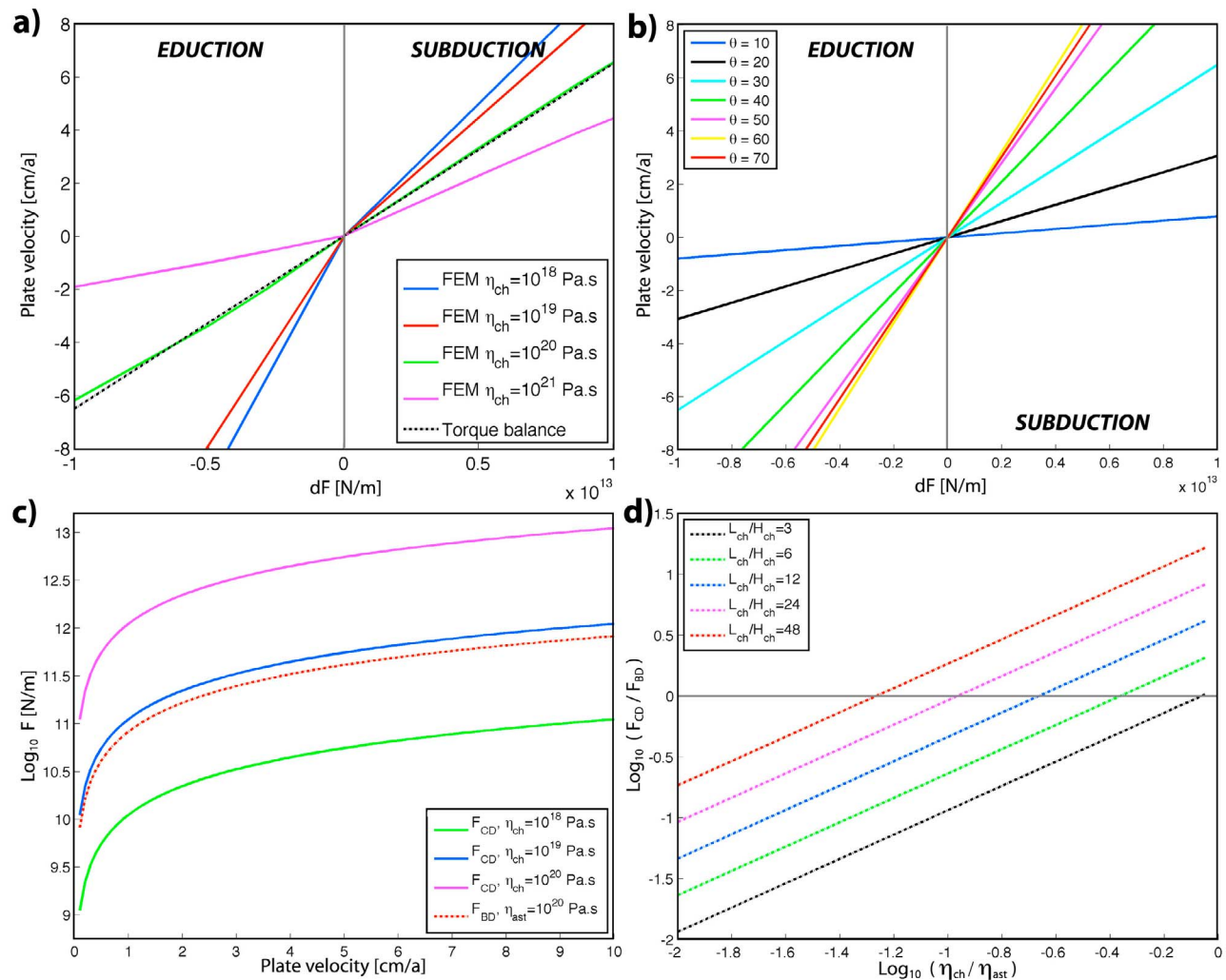
**Figure 9.** (a) Plate velocity for variable force difference (*dF*) (using $\eta_{ast} = 10^{20}$ Pa.s and $\theta = 30°$). The solid lines represent the solution obtained from the 2D simulations for different subduction channel viscosities ($\eta_{ch}$). The dotted line is the prediction of the torque balance approach for an isoviscous mantle. (b) Sensitivity of plate velocity to the slab dip angle for variable force difference values. This was computed using the torque balance model. (c) Magnitude of the basal drag (red) and channel drag forces (blue) estimated for our 2D setup as a function of plate velocity. These estimations assume a Couette flow in the asthenosphere and the subduction channel. (d) Efficiency of the subduction channel drag over the basal drag for various channel aspect ratios and channel/asthenosphere viscosity contrast.

each approach, the FE and torque balance results are in good agreement. The FE models confirm the result of the toque balance approach when the subduction channel's viscosity is equal to that of the asthenosphere (isoviscous case). Both approaches predict that eduction occurs if the buoyancy of the slab exceeds the ridge push force (*dF* < 0).

#### 6.1.1. Slab Dip

[23] The effect of the slab dip was investigated using the torque balance approach. We have used a constant asthenosphere viscosity of $10^{20}$ Pa.s and varied the slab dip from 10 to 70 degrees (Figure 9b). The slab dip angle shows a significant influence on the plate velocities. Plate velocities increase with increasing dip angle up to an optimal angle of ≈60 degrees (close to the results of *Stevenson and Turner*

[1977]). Over this critical dip angle value, the plates velocities decrease with increasing slab dip.

#### 6.1.2. Asthenosphere Viscosity

[24] The asthenosphere provides viscous resistance to slab penetration. This resistance can be decomposed in force acting parallel to the motion direction and a basal drag tangential to the slab face ($F_{BD}$). From the torque balance model, the slab velocity is inversely proportional to the asthenosphere viscosity. A viscosity increase of one order of magnitude will therefore produce a velocity decrease of the same magnitude. However, a more realistic model would also take into account effects of the slab bending [*Buffet*, 2006], the drag torque due to slab curvature, or the slab anchoring due to the upper plate motion [*Scholz and Campos*, 1995;

*Lallemand et al.*, 2008] which would also affect subduction/eduction rates. The magnitude of the basal drag force in or 2D can be estimated by considering a Couette flow in the mantle driven by the slab motion in such manner:

$$F_{BD} \propto \eta_{ast} V \frac{L_{Plate}}{H_{ast}}. \tag{11}$$

Using a plate length ($L_{Plate}$) of 1500 km and an asthenospheric channel thickness ($H_{ast}$) of 500 km, Figure 9c shows that the estimated magnitude of basal drag does not exceed $8 \times 10^{11}$ N/m even for plate velocities larger than 8 cm/y. This justifies that the basal drag force plays a minor role in our calculations.

### 6.1.3. Subduction Channel Viscosity

[25] Similarly to the basal drag force, a slab tangential force is also generated in the subduction channel ($F_{BD}$). Its influence on plate velocities can not be investigated by the isoviscous torque balance model, however the 2D simulations showed large sensitivity to this parameter (Figure 9a). At first order, the magnitude of this force may also be approximated from a simple Couette flow model driven by the subducting plate and leading to the expression:

$$F_{CD} \propto \eta_{ch} V \frac{L_{Channel}}{H_{Channel}}. \tag{12}$$

Estimated channel drag forces computed using a channel length ($L_{Channel}$ = 300 km) and thickness ($H_{Channel}$ = 15 km) corresponding to our 2D setup are depicted in Figure 9c. In the ideal case, the channel is considered to provide strong mechanical decoupling between the plates, and hence should not produce a strong drag force (e.g. Figure 9c with $\eta_{ch} = 10^{18}$ Pa.s). However, its magnitude is highly dependent on the channel viscosity and may overcome the basal drag force once the channel viscosity tends to the asthenosphere viscosity (e.g. Figure 9c with $\eta_{ch} = 10^{20}$ Pa.s). Another major parameter is the aspect ratio of the channel, Figure 9d shows the ratio of channel/basal drag force magnitudes for variable channel/asthenosphere viscosity ratio and channel aspect ratio. These results indicate that, in the case the channel undergoes strengthening processes and/or geometrical modifications (thickening/thinning), channel drag may largely overcome basal drag and might become a major force ($F_{CH} > 10^{12}$ N/m).

## 7. Discussion

### 7.1. Low Peak Temperature in the Exhumed Crust

[26] In our simulations, the reference model presented here fails at producing sufficiently large enough temperatures in the exhumed HP rocks compared to geological examples of HP and UHP rocks formed at corresponding extreme burial depths (T < 600 to 750°C). These low temperatures can be explained by the short residence time of subducted material at mantle depths which is limited by the onset of extensional processes within the orogen. An unrealistic low geotherm of less than 3 C/km during continental subduction is the result of this model. Hence, a fast (cold) subduction/collision is subject to a rapid burial and aborted by slab detachment. In this case, the main exhumation stage occurs after the detachment and the buried continental margin is educted

without reaching high temperatures. Since a fast convergence plate eduction models can only explain the exhumation of cold UHP rocks (T < 500°C), we expect that slower convergence rates are likely to produce and exhume UHP rocks with higher temperatures. Although our simulations take into account the thermomechanical feedback induced by viscous dissipation, the peak temperatures reached by the exhumed material are approximately 100°C too cold to match natural data. These results, comparable to those obtained in previous studies [*Yamato et al.*, 2008; *Stöckhert and Gerya*, 2005], tend to show that viscous dissipation may not explain common peak temperatures (T > 600°C) of exhumed HP and UHP rocks. In contrast to the results of *Li and Gerya* [2009] and *Li et al.* [2011], our simulations do not account for partial melting, this may potentially explain our low peak temperatures. We expect the heat advected by the partially molten upwellings and the heat released during crystallization of potential plutons to provide the missing ≈100°C. As material for discussion, we present additional subduction-collision models that were obtained following the same methodology as in the simulations presented above (i.e. without including any effect related to melting).

### 7.1.1. A Delamination-Eduction Model

[27] The models presented in Section 3 were designed in order to isolate the process of slab eduction. However, more realistic models of orogenic evolution may include delamination [*Bird*, 1978] or buoyant uplift [*Warren et al.*, 2008a, 2008b] linked to slab rollback. Figure 10a depicts the evolution of an initially slower continental collision (1.25 cm/y). The simulation runs for 40 My before continental subduction takes place. The burial stage lasts for about 10 My and the subducted crust is affected by delamination as soon as the continental crust reaches its maximum depth of burial (≈200 km). Most of the decompression occurs during the delamination period that lasts approximately 7 My before slab detachment eventually occurs triggering a late stage eduction event. As indicated by Figure 10b, the exhumed crust peak temperatures higher than in the case of pure eduction (≈660°C). Another feature of this delamination-eduction model is the flow of the extruded crust toward the foreland that leads to a stage of orogenic broadening, and the occurrence of a deep-seated thrust that likely to be exposed in the hinterland of the broadened mountain belt. The combination of delamination and eduction gives rise to the exhumation of HP-UHP rocks with peak temperatures of 500 to 650°C, more akin to natural examples, and we therefore regard this type of exhumation model as more realistic.

### 7.1.2. Subduction of a Thinned Continental Margin

[28] Similarly to boudinage instabilities [*Schmalholz et al.*, 2008], slab detachment has been demonstrated to be the result of a viscous necking instability in a power law fluid [*Schmalholz*, 2011]. We therefore expect our slab detachment to be sensitive to the geometry and the thermal state of the subducted margin (amplitude and wavelength of the initial perturbation). Figure 11a displays the time evolution of a model employing a thinned ocean-continent transition. Although, the initial convergence rate is prescribed similarly as for our reference model (5 cm/y), the presence of a stretched ocean-continent transition delays slab detachment and ultimately favors delamination. The distal part of the margin reaches a maximum depth larger than 200 km from where the delamination of the upper crust is initiated. As the
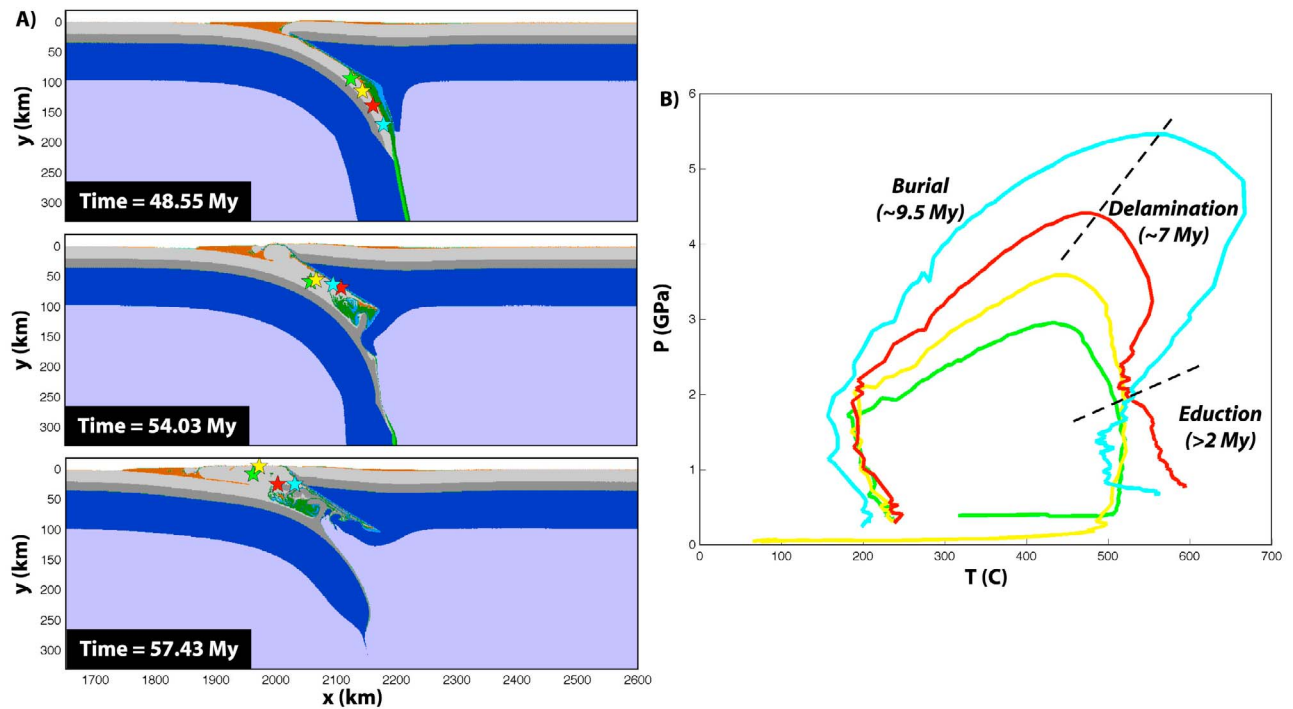
**Figure 10.** (a) Temporal evolution of the delamination/eduction model, the colored stars correspond to Lagrangian tracers used to record the pressure-temperature history of the subducted continental crust. (b) Pressure-temperature evolution of the Lagrangian tracers throughout the collision event.
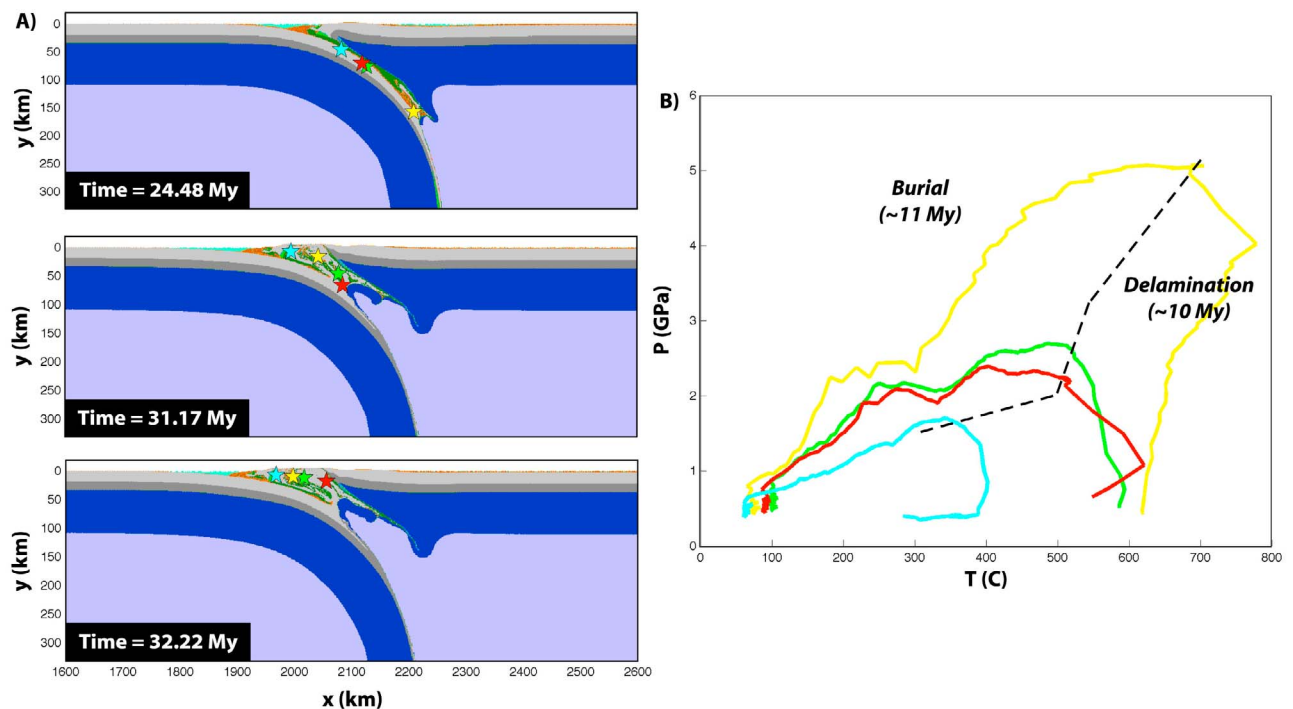
**Figure 11.** (a) Evolution of the thinned margin subduction model, this feature inhibits slab detachment at the timescale of the collision. The Lagrangian tracers used to record the pressure-temperature history of the subducted continental crust are denoted as colored stars. (b) PT paths corresponding to different initial locations within the passive margin.

delamination occurs (≈10 My), several nappes detach from the subducted margin. These buoyant nappes are emplaced adjacently stacked within the orogen and record significantly different PT histories (Figure 11b). This model is in agreement with previous studies [*Warren et al.*, 2008b; *Li et al.*, 2011; *Yamato et al.*, 2008] that showed that slab detachment is not a necessary factor for the exhumation of high pressure rocks and that the stage of continental collision does not exceed more than 10 My [*Yamato et al.*, 2008].

### 7.1.3. The Western Gneiss Region, Scandinavian Caledonides

[29] The idea of continental subduction and eduction following slab breakoff at the terminal stages of a Wilson cycle was put forward in order to explain the geological observations from the Scandian continent-continent collision in the Caledonides [*Andersen et al.*, 1991]. The collision produced one of the worlds largest HP-UHP terrains and the main characteristics of the vast Western Gneiss Region (WGR) are:

[30] 1. Protoliths of the HP-UHP rocks are Middle Proterozoic (≈1700 to 950 My) mostly orthogneisses [e.g., *Austrheim et al.*, 2003; *Tucker et al.*, 2004], and major parts of the WGR experienced granulite metamorphic conditions at ≈1 Ga [e.g., *Røhr et al.*, 2004; *Krabbendam et al.*, 2000].

[31] 2. The uppermost structural level of the WGR is a nearly intact Proterozoic crust, only affected by the Caledonian metamorphism and deformation near the basal Caledonian thrust [*Labrousse et al.*, 2010].

[32] 3. The WGR has a metamorphic field-gradient from 600°C at 1.8 GPa in the east to 750°C at 2.8 GPa in the west [e.g., *Young et al.*, 2007; *Hacker et al.*, 2010].

[33] 4. The HP-UHP metamorphism in the WGR lasted nearly 20 My (415 to 397 My [e.g., *Krogh et al.*, 2011]), whereas Scandian HP in the nappes is older up to 430 My [*Glodny et al.*, 2008].

[34] 5. There are no exposed major syn- to post-UHP-metamorphic thrusts [*Hacker et al.*, 2010], and a very large-scale extensional detachment zone separates the HP-UHP rocks in the footwall from lower grade nappes in the hanging wall.

[35] 6. The total duration of the Scandian continental collision was approximately 30 My (430 to 400 My) [*Andersen et al.*, 1990; *Corfu et al.*, 2006].

[36] The absence of large-scale structures perturbing the regional metamorphic zonation within the WGR suggests that it was buried and exhumed as a mostly intact slab (40000 km$^2$) of continental crust. Some very local extreme UHP occurrences recording 3 to 6 GPa (diamond, majoritic garnet and opx-eclogites) within the coesite-grade domains (see review by *van Roermund* [2009]) cannot be fitted to the regional metamorphic field gradient and probably needs alternative explanations [*Vrijmoed et al.*, 2009], which will not be discussed here. The eduction model presented in this study (Figure 5) results in a 2D structural geometry of the exhumed HP-UHP rocks, which is quite similar to observations in the WGR [*Andersen et al.*, 1991, Figure 2]. The duration since on-set of collision is 27 My (Figure 4b), also similar to the Caledonian analog. The HP-UHP rocks also constitute the lowermost observable structural level similar to what is observed in western Norway. There is no large-scale thrust below the UHP rocks, and there is a very large

extensional detachment above the HP-UHP rocks. The model presented in Figure 5, however, fails to reproduce the temperatures similar to those seen in the eclogites in the WGR by approximately 150 to 250°C [*Hacker et al.*, 2010; *Labrousse et al.*, 2004]. It is obvious that the reference eduction model used here is too cold to explain the WGR example in full. The alternative delamination-eduction model (Figure 10) also reproduces a number of the field characteristics, and the temperatures obtained are still lower (up to 100°C), but more comparable to those from the WGR. The main structural difference between the eduction and the delamination-eduction models is that the delamination stage produces a major thrust at mid-crustal levels, below the UHP rocks during exhumation (Figure 10). The presence of such thrust(s) has been postulated in several papers on the WGR [e.g., *Andersen et al.*, 1991; *Hacker et al.*, 2010], but the existence has not been verified by observation in the field. If present it must be covered by nappes in south-central Norway. Observations that argue against the presence of the deep thrust is that sedimentary cover to the autochthonous Proterozoic basement can be traced almost continuously along the basal thrust from the foreland below the nappes to the WGR in central south Norway. Considering all available geological and geophysical observations [*Andersen*, 1998], a geomechanical model combining delamination with slab breakoff and eduction provides the best quantifiable model for exhumation of the HP-UHP rocks in the WGR.

## 7.2. Limitations of the Density Model

[37] Although we did not explicitly consider the effect of phase transitions occurring within the continental crust, the crustal densities were calculated according to the transient pressure-temperature conditions. The equation of state (see Appendix A) allows the upper crustal density to smoothly vary between 2700 to 2850 kg/m$^3$ whereas lower crust density ranges between 2800 to 2950 kg/m$^3$ (Figure 4). Both density changes related to either phase changes or the equation of state were considered to be instantaneous and reversible. Natural observation indicates that reaction kinetics can be slow and can lead to partial prograde phase transformations [*Krabbendam et al.*, 2000] and neglecting this effect might lead to an overestimation of the crust density on the prograde path. This would have the effect of overvaluing the buoyancy of the crust and could potentially reduce the peak burial depth of continental crust prior to slab detachment. On the other hand, retrograde density changes may lead to an underestimation of the crust density and therefore overrating the root buoyancy force in the later stages of eduction.

## 7.3. Comparison With the Models of Coherent Nappe Exhumation

[38] The models proposed by *Chemenda et al.* [1995, 1996, 1997] involved decoupling of the subducting crust from the mantle lithosphere and exhumation of the coherent nappe by faulting of the crust. Although overall kinematics of exhumation resembles the eduction model, the dynamics of these models are different. In *Chemenda et al.* [1995], the buried crust decouples from the mantle lithosphere, implying weak mechanical coupling at the Moho. Similarly to our model, the exhumation of the nappe is coherent. The exhumation process differ by the fact that it requires the presence

of a thrust on the lower plate which is not required by the education model. A main similarity between those models is the presence of a normal sense shear zone in the vicinity of the suture. In our simulations, the main normal shear zone is produced consequently to slab detachment and eduction. Despite slab breakoff occurred in the experiments of *Boutelier et al.* [2004], no eduction was observed because of two major reasons: (1) the crust had already delaminated from the mantle at breakoff time, preventing coherent lithospheric-scale motion, (2) the system was subject to a continued kinematic push.

### 7.4. Dimensionality and Plate Motions

[39] Our two-dimensional models do not take into account effects related to three dimensional flow in the mantle. We can expect that the toroidal flow component can have a strong influence on subduction-collision systems. A consequence is the tendency for subduction to roll back, leading to a more decoupled, or retreating, style of collision [*Husson et al.*, 2009; *Stegman et al.*, 2006]. The plate eduction endmember is triggered by slab detachment, recent three-dimensional studies of slab detachment [*Burkett and Billen*, 2011; *van Hunen and Allen*, 2011] show that the tearing of the slab can happen in an inhomogeneous manner along the trench direction. We thus expect that plate eduction will take place progressively in the along trench direction following the detachment of the slab at depth. This direction of slab tearing should also control the timing and location of emplacement of the exhumed high pressure nappes as well as surface uplift and filling of the adjacent basins. Another 3D aspect of the force balance change related to slab detachment is the possibility to trigger abrupt changes in plate motion [*Austermann et al.*, 2011]. In our 2D study, the main consequence of the slab pull is the partial eduction of the subducted slab from the subduction zone. Our results shows that a lower plate horizontal displacement on the order of 100 km can result from eduction. In three dimensions, finite-width slabs associated with progressive (along trench) slab detachment may lead to changes in plate motion directions and potentially to rotations. On the other hand, we could also expect that plate rotations, which can be triggered by oblique continental collision [*Bellhasen et al.*, 2003] can strongly affect slab detachment [*van Hunen and Allen*, 2011] and potentially help and/or trigger plate eduction in some specific conditions. Another simplification of our 2D results relies on the fact that detachment results in a total loss of the slab pull force. In three-dimensions, we may expect that slab portions might remain attached in the along-trench direction (along strike coupling) and provide additional pull force. The amount of eduction will consequently decrease according to the magnitude of pull that can be transmitted along strike. Variations of slab width may also occur during subduction [*Guillaume et al.*, 2010] and might strongly perturb the subduction force leading to variations of plate velocities, such effect may promote slab rollback and detachment as well as the development of slab tear faults [*Wortel et al.*, 2009].

### 8. Conclusions

[40] The plate eduction model is characterized by the inversion of the subduction plane within continental collision zones. This mechanism is likely to take place after slab detachment has occurred and eliminated the effect of slab pull. Our two-dimensional study demonstrates that this model can partly explain the exhumation of buried continental crust and orogenic extension. Models that isolate the plate eduction mechanism lead to quasi adiabatic decompression of the buried crust ($\approx 2$ GPa) in a timespan of 5 My. The coherent extraction of the slab from the subduction zone results in localized extensional strain within the subduction channel. This response to slab detachment is accompanied by the flattening of the slab and the build up of topography on the lower plate. We have derived scaling laws that enable the prediction of the lower plate velocity that is subjected to eduction. The plate velocity is function of the buoyancy of the previously subducted continental crust and of the lateral force that is exerted on the collision zone (e.g. ridge push). Asthenosphere and subduction channel viscosity mantle have a first order influence on the rate of eduction and allow eduction if their respective magnitudes are lower than $10^{22}$ and $10^{21}$ Pa.s. Eduction subsequent to slab detachment can occur in combination to other geodynamic processes (e.g. slab retreat) and may play a significant role in the geodynamic evolution of collision zones.

### Appendix A: Numerical Code Description

[41] The thermomechanical code I2VIS solves the two-dimensional steady state Stokes equations and heat conservation equation using the finite difference/marker-in-cell method [*Gerya and Yuen*, 2003a; *Gerya*, 2010]:

$$\frac{\partial \sigma_{ij}}{\partial x_j} = -\rho g_i \qquad (A1)$$

$$\frac{\partial v_i}{\partial x_i} = 0 \qquad (A2)$$

$$\frac{\partial}{\partial x_i}\left(k\frac{\partial T}{\partial x_i}\right) = -\rho C_p \frac{DT}{Dt} - H \qquad (A3)$$

where $x_j$ represents the spatial coordinates, $\rho$, the material density (kg/m$^3$), $k$, the thermal conductivity (W/m/K), $C_p$, the specific heat capacity (J/kg) and $H$ (J/m$^3$/s), the contribution of the different heat sources (radiogenic, shear, and adiabatic heating). The density and heat capacity of each lithology are functions of both pressure $P$ (Pa) and temperature $T$ (K). The oceanic crust, lithospheric and asthenospheric densities are pre-computed via Gibbs free energy minimization and updated at each timestep. The densities of continental crust rocks are calculated via the equation of state:

$$\rho = \rho_0\left(1 - \beta(T - 298.15)\right)\left(1 + \alpha\left(P \times 10^{-8} - 10^{-3}\right)\right) \qquad (A4)$$

where $\rho_0$ corresponds to the reference density (2700 kg/m$^3$ for the upper crust and 2800 kg/m$^3$ for the lower crust), $\beta$ to the isothermal compressibility (0.5 1/K for the crust) and $\alpha$ to the thermal expansivity (1.5 1/kbar for the crust). The thermal conductivity $k$ depends on the temperature [*Clauser and Huenges*, 1995], the functions used to evaluate $k$ are listed in Table 1.

[42] The mechanical solver uses a viscous formulation and the deviatoric stress tensor $\sigma_{ij}$ relates to the material viscosity $\eta$ and the rate of deformation $\dot{\epsilon}_{ij}$ via:

$$\sigma_{ij} = 2\eta\dot{\epsilon}_{ij} = \eta_{\text{eff}}\left(\frac{\partial v_i}{\partial x_j} + \frac{\partial v_j}{\partial x_i}\right) \quad (A5)$$

The different lithologies deform according to a visco-plastic rheology. At stresses larger than 30 kPa, most of the flow occurs in the dislocation creep regime [*Turcotte and Schubert*, 1982] and depends on the second invariant of the strain rate tensor ($\dot{\epsilon}_{\text{II}}$), the temperature and the pressure [*Ranalli*, 1995]. The effective viscosity corresponding to a dislocation creep regime is calculated as following:

$$\eta_{\text{creep}} = \eta_0^{\frac{1}{n}}\dot{\epsilon}_{\text{II}}^{\frac{1-n}{2n}} \exp\left(\frac{E_a + PV_a}{nRT}\right) \quad (A6)$$

where $n$ is the stress exponent, $\eta_0$, the reference viscosity ($\text{Pa}^n$.s), $E_a$, the activation energy (J), $V_a$, the activation volume (J/bar) and R, the gas constant (8.314472 J/mol/K).

[43] Mohr-Coulomb (or Drucker-Prager) plasticity act as a stress limiter in the regions where the second stress invariant ($\sigma_{\text{II}}$) exceeds the material yield stress. The yield stress depends on the pressure, the cohesion $C$ (MPa), and the internal friction angle $\phi$. The stress is limited via local viscosity reductions such as

$$\eta_{\text{creep}} \leq \frac{C + P\sin(\phi)}{2\sqrt{\dot{\epsilon}_{\text{II}}}} \quad (A7)$$

In the mantle, at sufficiently high stress and low temperature, Peierls plasticity may be the dominant deformation mechanism [*Evans and Goetze*, 1979; *Kameyama et al.*, 1999; *Raterron et al.*, 2004; *Katayama and Karato*, 2008]. This regime has exponential dependance on the second stress invariant and can therefore act as a strong weakening mechanism in the lithospheric mantle. The effective viscosity corresponding to the Peierls creep regime is formulated as:

$$\eta_{\text{Peierls}} = \frac{1}{A_{\text{Peierls}}\sigma_{\text{II}}} \exp\left[\left(\frac{E_a - PV_a}{RT}\right)\left(1 - \left(\frac{\sigma_{\text{II}}}{\sigma_{\text{Peierls}}}\right)^k\right)^q\right] \quad (A8)$$

In our simulations, this mechanism becomes active when the Peierls viscosity $\eta_{Peierls}$ is inferior to the creep viscosity $\eta_{creep}$. We use the dry olivine parameters $A_{Peierls} = 10^{7.8} \times 10^{-12}$ and $\sigma_{Peierls} = 9.1$ GPa [*Evans and Goetze*, 1979]. The viscosity is limited such that $10^{18} < \eta < 10^{25}$ Pa.s.

[44] The model's surface $h$ (air/crust interface) evolves following a gross-scale erosion-sedimentation law [*Gerya and Yuen*, 2003b; *Gerya*, 2010]:

$$\frac{\partial h}{\partial t} = v_y - v_x\frac{\partial h}{\partial x} - \dot{e} + \dot{s} \quad (A9)$$

where $v_y$ and $v_x$ are the uplift and advection velocity (m/s) predicted by the tectonic model. $\dot{e}$ and $\dot{s}$ represent prescribed erosion and sedimentation rates (m/s), they are set to 0.1 mm/y in our reference run. Erosion is active above a reference altitude of 1 km whereas sedimentation takes place at depths below $-1$ km.

[45] The result of the calculation of the fluid velocity obtained on the Eulerian grid and is interpolated to the Lagrangian markers, the advection equation is the solved explicitly by a coordinate update of the Lagrangian markers:

$$x_j^{t+1} = x_j^t + \Delta t\, v^t \quad (A10)$$

where $v^t$ corresponds to the marker velocity computed vi 4th order (in space) Runge-Kutta scheme, $\Delta t$ represent the value of the timestep at the current time integration.

## References

Andersen, T. B. (1998), Extensional tectonics in the Caledonides of southern Norway: An overview, *Tectonophysics*, *285*, 333–351.

Andersen, T. B., and B. Jamtveit (1990), Uplift of deep crust during orogenic extensional collapse: A model based on field studies in the Sogn-Sunnfjord region of Western Norway, *Tectonics*, *9*(4), 1097–1111.

Andersen, T. B., K. P. Skjerlie, and H. Furnes (1990), The Sunnfjord Melange, evidence of Silurian ophiolite accretion in the West Norwegian Caledonides, *J. Geol. Soc.*, *147*, 59–68.

Andersen, T. B., B. Jamtveit, J. F. Dewey, and E. Swensson (1991), Subduction and eduction of continental crust: Major mechanisms during continent-continent collision and orogenic extensional collapse, a model based on the south Norwegian Caledonides, *Terra Nova*, *3*, 303–310.

Andrews, E. R., and M. I. Billen (2009), Rheologic controls on the dynamics of slab detachment, *Tectonophysics*, *464*(1–4), 60–69.

Austermann, J., Z. Ben-Avraham, P. Bird, O. Heidbach, G. Schubert, and J. M. Stock (2011), Quantifying the forces needed for the rapid change of Pacific plate motion at 6 Ma, *Earth Planet. Sci. Lett.*, *307*, 289–297.

Austrheim, H., F. Corfu, I. Bryhni, and T. B. Andersen (2003), The Proterozoic Hustad igneous complex: A low strain enclave with a key to the history of the Western Gneiss Region of Norway, *Precambrian Res.*, *120*, 149–175.

Baumann, C., T. V. Gerya, and J. A. D. Connolly (2009), Numerical modelling of sponaneous slab breakoff dynamics during continental collision, in *Advances in Interpretation of Geological Processes: Refinement of Multi-scale Data and Integration in Numerical Modelling*, edited by M. Spalla, A. Marotta, and G. Gosso, *Geol. Soc. Spec. Publ.*, *322*, 99–114.

Beaumont, C., R. A. Jamieson, M. H. Nguyen, and B. Lee (2001), Himalayan tectonics explained by extrusion of a low-viscosity crustal channel coupled to focused surface denudation, *Nature*, *414*(6865), 738–742.

Beaumont, C., R. A. Jamieson, M. H. Nguyen, and S. Medvedev (2004), Crustal channel flows: 1. Numerical models with implications to the tectonics of the Himalayan-Tibetan orogen, *J. Geophys. Res.*, *109*, B06406, doi:10.1029/2003JB002809.

Beaumont, C., R. A. Jamieson, M. H. Nguyen, and S. Ellis (2006), Crustal flow modes in large hot orogens, in *Channel Flow, Ductile Extrusion and Exhumation in Continental Collision Zones*, edited by R. D. Law, M. P. Searle, and L. Godin, *Geol. Soc. Spec. Publ.*, *268*, 91–145.

Bellhasen, N., C. Faccenna, F. Funiciello, J. M. Daniel, and L. Jolivet (2003), Why did Arabia separate from Africa? Insights from 3-D laboratory experiments, *Earth Planet. Sci. Lett.*, *216*, 365–381.

Bialas, R. W., F. Funiciello, and C. Faccenna (2011), Subduction and exhumation of continental crust: Insights from laboratory models, *Geophys. J. Int.*, *184*, 43–64.

Bird, P. (1978), Initiation of intracontinental subduction in the Himalaya, *J. Geophys. Res.*, *83*(B10), 4975–4987.

Boutelier, D., A. Chemenda, and C. Jorand (2004), Continental subduction and exhumation of high-pressure rocks: Insights from thermo-mechanical laboratory modelling, *Earth Planet. Sci. Lett.*, *222*, 209–216.

Brueckner, H. K. (2009), Subduction of continental crust, the origin of post-orogenic granitoids (and anorthosites?) and the evolution of Fennoscandia, *J. Geol. Soc.*, *166*, 753–762.

Brueckner, H. K., and H. L. M. van Roermund (2004), Dunk tectonics: A multiple subduction/eduction model for the evolution of the Scandinavian Caledonides, *Tectonics*, *23*, TC2004, doi:10.1029/2003TC001502.

Brun, J. P., and C. Facenna (2008), Exhumation of high-pressure rocks driven by slab rollback, *Earth Planet. Sci. Lett.*, *272*, 1–7.

Buiter, S. J. H., R. Govers, and M. J. R. Wortel (2002), Two-dimensional simulation of surface deformation caused by slab detachment, *Tectonophysics*, *354*(3–4), 192–210.

Buffet, B. A. (2006), Plate force due to bending at subduction zones, *J. Geophys. Res.*, *111*, B09405, doi:10.1029/2006JB004295.

Burkett, E. R., and M. I. Billen (2011), Three-dimensionality of slab detachment due to ridge-trench collision: Laterally simultaneous boudinage versus tear propagation, *Geochem. Geophys. Geosyst.*, *11*, Q11012, doi:10.1029/2010GC003286.

Chemenda, A. I., M. Mattauer, J. Malavieille, and A. Bokun (1995), A mechanism for syn-collisional rock exhumation and associated normal faulting: Results from physical modelling, *Earth Planet. Sci. Lett.*, *132*, 225–232.

Chemenda, A. I., M. Mattauer, and A. Bokun (1996), Continental subduction and a mechanism for exhumation of high-pressure metamorphic rocks: New modelling and field data from Oman, *Earth Planet. Sci. Lett.*, *143*, 172–182.

Chemenda, A. I., P. Matte, and V. Sokolov (1997), A model of Paleozoic obduction and exhumation of high-pressure/low-temperature rocks in the southern Urals, *Tectonophysics*, *276*, 217–227.

Clauser, C., and E. Huenges (1995), Thermal conductivity of rocks and minerals, in *Rock Physics and Phase Relations*, *AGU Ref. Shelf* vol. 3, edited by T. J. Ahrens, pp. 105–126, AGU, Washington, D. C.

Cloos, M., and R. L. Shreve (1988), Subduction-channel model of prism accretion, melange formation, sediment subduction, and subduction erosion at convergent plate margins: 1. Background and description, *Pure Appl. Geophys.*, *128*(3–4), 455–500.

Corfu, F., T. H. Torsvik, T. B. Andersen, L. D. Ashwal, D. M. Ramsay, and R. J. Roberts (2006), Early Silurian mafic-ultramafic and granitic plutonism in contemporaneous flysch, Magerøy, northern Norway: U-Pb ages and regional significance, *J. Geol. Soc.*, *163*, 291–301.

Crameri, F., H. Schmeling, G. J. Golabek, T. Duretz, R. Orendt, S. J. H. Buiter, D. A. May, B. J. P. Kaus, T. V. Gerya, and P. J. Tackley (2012), A comparison of numerical surface topography calculations in geodynamic modelling: An evaluation of the 'sticky air' method, *Geophys. J. Int.*, *189*, 38–54.

Davies, H. J., and F. von Blanckenburg (1995), Slab breakoff: A model of lithosphere detachment and its test in the magmatism and deformation of collisional orogens, *Earth Planet. Sci. Lett.*, *129*(1–4), 85–102.

Dixon, J. M., and E. Farrar (1980), Ridge subduction, eduction, and the neogene tectonics of southwestern North America, *Tectonophysics*, *67*, 81–99.

Duretz, T., T. V. Gerya, and D. A. May (2011), Numerical modelling of spontaneous slab breakoff and subsequent topographic response, *Tectonophysics*, *502*(1–2), 244–256, doi:10.1016/j.tecto.2010.05.024.

Dvorkin, J., A. Nur, G. Mavko, and Z. Ben-Avraham (1993), Narrow subducting slabs and the origin of backarc basins, *Tectonophysics*, *227*, 63–73.

Evans, B., and C. Goetze (1979), Temperature variation of hardness of olivine and its implication for polycristalline yield stress, *J. Geophys. Res.*, *84*, 5505–5524.

Fossen, H. (2000), Extensional tectonics in the Caledonides: Synorogenic or postorogenic?, *Tectonics*, *19*(2), 213–224.

Froitzheim, N., J. Pleuger, S. Roller, and T. Nagel (2003), Exhumation of high- and ultrahigh-pressure metamorphic rocks by slab extraction, *Geology*, *31*, 925–928.

Gerya, T. V. (2010), *Introduction to Numerical Geodynamic Modelling*, 345 pp., Cambridge Univ. Press, Cambridge, U. K.

Gerya, T. V., and D. A. Yuen (2003a), Charaterictics-based marker method with conservative finite-difference schemes for modeling geological flows with strongly variable transport properties, *Phys. Earth Planet. Inter.*, *140*(4), 293–318.

Gerya, T. V., and D. A. Yuen (2003b), Rayleigh-Taylor instabilities from hydration and melting propel 'cold plumes' at subduction zones, *Earth Planet. Sci. Lett.*, *212*(1–2), 47–62.

Gerya, T. V., B. Stoeckhert, and L. L. Perchuk (2002), Exhumation of high-pressure metamorphic rocks in a subduction channel: A numerical simula- tion, *Tectonics*, *21*(6), 1056, doi:10.1029/2002TC001406.

Gerya, T. V., D. A. Yuen, and W. Maresch (2004), Thermomechanical modelling of slab detachment, *Earth Planet. Sci. Lett.*, *226*(1–2), 101–116.

Glodny, J., A. Kühn, and H. Austrheim (2008), Geochronology of fluid-induced eclogite and amphibolite facies metamorphic reactions in a subduction-collision system, Bergen Arcs, Norway, *Contrib. Mineral. Petrol.*, *156*, 27–48.

Guillaume, B., F. Funiciello, C. Faccenna, J. Martinod, and V. Olivetti (2010), Spreading pulses of the Tyrrhenian Sea during the narrowing of the Calabrian slab, *Geology*, *38*(9), 819–822.

Hacker, B. R., T. B. Andersen, S. Johnston, A. R. C. Kylander-Clark, E. M. Peterman, E. O. Walsh, and D. Young (2010), High-temperature deformation during continental-margin subduction and exhumation: The ultrahigh-pressure Western Gneiss Region of Norway, *Tectonophysics*, *480*(1–4), 149–171.

Huet, B., L. Le Pourhiet, L. Labrousse, E. Burov, and L. Jolivet (2010), Post-orogenic extension and metamorphic core complexes in a heterogeneous crust: The role of crustal layering inherited from collision: Application to the Cyclades (Aegean domain), *Geophys. J. Int.*, *184*(2), 611–625.

Husson, L., J.-P. Brun, P. Yamato, and C. Faccenna (2009), Episodic slab rollback fosters exhumation of HP–UHP rocks, *Geophys. J. Int.*, *179*, 1292–1300.

Janák, M., N. Froitzheim, M. Vrabec, E. J. Krogh Ravna, and J. C. M. De Hoog (2006), Ultrahigh-pressure metamorphism and exhumation of garnet peridotite in Pohorje, Eastern Alps, *J. Metamorph. Geol.*, *24*(1), 19–31, doi:10.1111/j.1525-1314.2005.00619.x.

Kameyama, M., D. A. Yuen, and S.-I. Karato (1999), Thermal-mechanical effects of low-temperature plasticity (the Peierls mechanism) on the deformation of viscoelastic shear zone, *Earth Planet. Sci. Lett.*, *168*(1–2), 159–172.

Katayama, I., and S.-I. Karato (2008), Rheological structure and deformation of subducted slabs in the mantle transition zone: Implications for mantle circulation and deep earthquakes, *Phys. Earth Planet. Inter.*, *168*(3–4), 125–133.

Kaus, B. (2010), Factors that control the angle of shear bands in geodynamic numerical models of brittle deformation, *Tectonophysics*, *484*(1–4), 36–47.

Krabbendam, M., A. Wain, and T. B. Andersen (2000), Pre-Caledonian granulite and gabbro enclaves in the Western Gneiss Region, Norway: Indications of incomplete transition at high pressure, *Geol. Mag.*, *137*, 235–255.

Krogh, T. E., S. L. Kamo, P. Robinson, M. P. Terry, and K. Kwok (2011), U-Pb zircon geochronology of eclogites from the Scandian Orogen, northern Western Gneiss Region, Norway: 14–20 million years between eclogite crystallization and return to amphibolite- facies conditions, *Can. J. Earth Sci.*, *48*, 441–472.

Labrousse, L., L. Jolivet, T. B. Andersen, P. Agard, H. Maluski, and U. Schärer (2004), Pressure-temperature-time deformation history of the exhumation of ultra-high pressure rocks in the Western Gneiss Region, Norway, in *Gneiss Domes in Orogeny*, vol. 380, edited by D. L. Whitney, C. Teyssier, and C. S. Siddoway, pp. 155–185, Geol. Soc. Am., Boulder, Colo.

Labrousse, L., G. Hetény, H. Raimbourg, L. Jolivet, and T. B. Andersen (2010), Initiation of crustal-scale thrusts triggered by metamorphic reactions at depth: Insights from a comparison between the Himalayas and Scandinavian Caledonides, *Tectonics*, *29*, TC5002, doi:10.1029/2009TC002602.

Lallemand, S., A. Heuret, C. Faccenna, and F. Funiciello (2008), Subduction dynamics as revealed by trench migration, *Tectonics*, *27*, TC3014, doi:10.1029/2007TC002212.

Li, Z., and T. V. Gerya (2009), Polyphase formation and exhumation of high- to ultrahigh-pressure rocks in continental subduction zone: Numerical modeling and application to the sulu ultrahigh-pressure terrane in eastern China, *J. Geophys. Res.*, *114*, B09406, doi:10.1029/2008JB005935.

Li, Z. H., Z. Q. Xu, and T. V. Gerya (2011), Flat versus steep subduction: Contrasting modes for the formation and exhumation of high- to ultrahigh-pressure rocks in continental collision zones, *Earth Planet. Sci. Lett.*, *301*, 65–77.

Lister, G., M. A. Forster, and T. J. Rawling (2001), Episodicity during orogenesis, *Geol. Soc. Spec. Publ.*, *184*, 89–113.

Manea, V., M. Manea, V. Kostoglodow, and G. Sewell (2006), Intraslab seismicity and thermal stress in the subducted Cocos plate beneath central Mexico, *Tectonophysics*, *420*, 389–408.

McKenzie D. P. (1969), Speculations on the consequences and causes of plate motions, *Geophys. J. R. Astron. Soc.*, *18*, 1–32.

Mishin, Y. A., T. V. Gerya, J.-P. Burg, and J. A. Connolly (2008), Dynamics of double subduction: Numerical modeling, *Phys. Earth Planet. Inter.*, *171*(1–4), 280–295, doi:10.1016/j.pepi.2008.06.012.

Ranalli, G. (1995), *Rheology of the Earth*, 2nd ed., Chapman and Hall, London.

Raterron, P., Y. Wu, D. J. Weidner, and J. Chen (2004), Low-temperature olivine rheology at high pressure, *Phys. Earth Planet. Inter.*, *145*, 149–159.

Rey, P., J. P. Burg, and M. Casey (1997), The Scandinavian Caledonides and their relationship to the Variscan belt, *Geol. Soc. Spec. Publ.*, *121*, 179–200.

Røhr, T. S., F. Corfu, H. Austrheim, and T. B. Andersen (2004), Sveconorwegian U-Pb zircon and monazite ages of granulite-facies

rocks, Hisarøya Gulen, Western Gneiss Region, *Norweg. J. Geol.*, *84*, 251–256.

Schellart, W. P., G. Lister, and V. G. Toy (2006), A Late Cretaceous and Cenozoic reconstruction of the Southwest Pacific region: Tectonics controlled by subduction and slab rollback processes, *Earth Sci. Rev.*, *76*, 191–233.

Schlindwein, V., and W. Jokat (2000), Post-collisional extension of the East Greenland Caledonides: A geophysical perspective, *Geophys. J. Int.*, *140*, 559–567.

Schmalholz, S. M. (2011), A simple analytical solution for slab detachment, *Earth Planet. Sci. Lett.*, *304*(1–2), 45–54.

Schmalholz, S. M., D. W. Schmid, and R. C. Fletcher (2008), Evolution of pinch-and-swell structures in a power-law layer, *J. Struct. Geol.*, *30*(5), 649–663.

Schmeling, H., et al. (2008), A benchmark comparison of spontaneous subduction models: Towards a free surface, *Phys. Earth Planet. Inter.*, *171*(1–4), 198–223.

Schneider, D. A., S. J. Zahniser, J. M. Glascock, S. M. Gordon, and M. Manecki (2006), Thermochronology of the West Sudetes (Bohemian Massif): Rapid and repeated eduction in the Eastern Variscides, Poland and Czech Republic, *Am. J. Sci.*, *306*, 846–873.

Scholz, C. H., and J. Campos (1995), On the mechanism of seismic decoupling and back arc spreading at subduction zones, *J. Geophys. Res.*, *100*(B11), 103–115.

Stegman, D. R., J. Freeman, W. P. Schellart, L. Moresi, and D. A. May (2006), Influence of trench width on subduction hinge retreat rates in 3-D models of slab rollback, *Geochem. Geophys. Geosyst.*, *7*, Q03012, doi:10.1029/2005GC001056.

Stevenson, D. J., and J. S. Turner (1977), Angle of subduction, *Nature*, *270*(1–2), 334–336.

Stöckhert, B., and T. V. Gerya (2005), Pre-collisional high pressure metamorphism and nappe tectonics at active continental margins: A numerical simulation, *Terra Nova*, *17*, 102–110.

Tucker, R. D., P. Robinson, A. Solli, D. G. Gee, T. Thorsnes, T. E. Krogh, Ø. Nordgulen, and M. E. Bickford (2004), Thrusting and extension in the Scandian Hinterland, Norway: New U-Pb ages and tectonostratigraphic evidence, *Am. J. Sci.*, *304*, 477–532.

Turcotte, D. L., and G. Schubert (1982), *Geodynamics: Application of Continuum Physics to Geological Problems*, John Wiley, New York.

van Hunen, J., and M. B. Allen (2011), Continental collision and slab break-off: A comparison of 3-D numerical models with observations, *Earth Planet. Sci. Lett.*, *302*(1–2), 27–37.

van Roermund, H. (2009), Recent progress in Scandian ultrahigh-pressure metamorphism in the northernmost domain of the Western Gneiss Complex, SW Norway: Continental subduction down to 180–200 km depth, *Am. J. Sci.*, *166*(4), 739–751.

Vanderhaeghe, O., and C. Teyssier (2001), Partial melting and flow of orogens, *Tectonophysics*, *342*(3–4), 451–472.

Vrijmoed, J. C., Y. Y. Podladchikov, T. B. Andersen, and E. H. Hartz (2009), An alternative model for ultra-high pressure in the Svartberget Fe-Ti garnet-peridotite, Western Gneiss Region, Norway, *Eur. J. Mineral.*, *21*(6), 1119–1133.

Warren, C. J., C. Beaumont, and R. A. Jamieson (2008a), Modelling tectonic styles and ultra-high pressure (UHP) rock exhumation during the transition from oceanic subduction to continental collision, *Earth Planet. Sci. Lett.*, *267*, 129–245.

Warren, C. J., C. Beaumont, and R. A. Jamieson (2008b), Formation and exhumation of ultra-high-pressure rocks during continental collision: Role of detachment in the subduction channel, *Geochem. Geophys. Geosyst.*, *9*, Q04019, doi:10.1029/2007GC001839.

Wortel, R., R. Govers, and W. Spakman (2009), Continental collision and the STEP-wise evolution of convergent plate boundaries: From structure to dynamics, in *Subduction Zones Geodynamics*, *Front. Earth Sci.*, edited by S. Lallemand and F. Funiciello, pp. 47–59, Springer, Berlin.

Yamato, P., E. Burov, P. Agard, L. Le Pourhiet, and L. Jolivet (2008), HP-UHP exhumation during slow continental subduction: Self-consistent thermodynamically and thermomechanically coupled model with application to the Western Alps, *Earth Planet. Sci. Lett.*, *271*(1–4), 63–74.

Young, D. J., B. R. Hacker, T. B. Andersen, and F. Corfu (2007), Prograde amphibolite facies to ultrahigh-pressure transition along Nordfjord, western Norway: Implications for exhumation tectonics, *Tectonics*, *26*, TC1007, doi:10.1029/2004TC001781.